

Received: 2 July 2010 – Accepted: 7 December 2010 – Published: 17 December 2010

Correspondence to: L. Laakso (lauri.laakso@iki.fi)

Published by Copernicus Publications on behalf of the European Geosciences Union.

30692

ACPD

10, 30691–30729, 2010

**South African
EUCAARI –
measurements**

L. Laakso et al.

Title Page

Abstract

Introduction

Conclusions

References

Tables

Figures

⏪

⏩

◀

▶

Back

Close

Full Screen / Esc

Printer-friendly Version

Interactive Discussion



Abstract

In this paper, new long-term measurements of chemical composition and physical properties of atmospheric aerosols carried out on the eastern brink of the heavily polluted Highveld area in South Africa are introduced. As expected, a high variability of aerosol properties was observed. Optical properties of aerosol particles were found to be closely correlated with particulate mass and number concentration in the case of polluted air masses. In contrast, in clean conditions there was no clear connection between optical properties and aerosol number concentration due to the presence of multiple sources including new particle formation.

1 Introduction

The direct and indirect radiative effects of aerosol particles constitute the largest uncertainty in current radiative forcing estimates of the Earth's climate system (Foster et al., 2007; Hansen et al., 2007). In order to reduce the uncertainties associated with atmospheric aerosols in the climate system, detailed information on the temporal and spatial variability of different aerosol properties are needed. Such information can be obtained from a combination of model simulations, remote sensing and continuous in-situ aerosol measurements.

Over the continental Southern Hemisphere, long-term aerosol measurements are limited to very few field studies (Jayaratne and Verma, 2001; Swap et al., 2003; Laakso et al., 2006; Suni et al., 2008; Rissler et al., 2006). On the African continent south of the equatorial region, number concentrations and optical properties of submicron aerosol particles have mainly been investigated during the SAFARI 1992 and SAFARI 2000 measurement campaigns (Swap et al., 2003; Ross et al., 2003). These campaigns highlighted the importance of regional circulation, seasonal pollutant variation and multiple inversion layers (Garstang et al., 1996). These authors also pointed out that the atmospheric aerosol particle population originates from a mixture of natural

South African EUCAARI – measurements

L. Laakso et al.

Title Page

Abstract

Introduction

Conclusions

References

Tables

Figures



Back

Close

Full Screen / Esc

Printer-friendly Version

Interactive Discussion



and anthropogenic emission sources, such as domestic burning, wild fires and industry.

Recently, Laakso et al. (2008) reported the annual behaviour of the sub-micron particle number concentration and associated new particle formation in a clean background savannah environment in South Africa, but the observations did not include measurements of aerosol optical properties.

The observations described in this study take place on Highveld in Central South Africa. This area is among the top five NO₂ emission hotspots in the world and is also a significant source of CO₂, SO₂ and sulphate particles (Held, 1996; Fleming and van der Merwe, 2004).

The industrial emissions from this area, along with other regional emissions and intense solar radiation, create a highly reactive pollution mixture (Swap et al., 2003).

As a result, reactive gases are rapidly converted into more oxidized and low-volatile compounds that produce secondary aerosols via nucleation and condensation. These particles grow to accumulation mode sizes and mix with particles from primary emissions. Due to their long lifetime, these accumulation mode particles can be transported across the Indian Ocean, as far as Australia (Wenig et al., 2002), thereby affecting the radiative balance over large areas.

Due to its global importance, Highveld was chosen as one of the EUCAARI project measurement areas outside Europe (Kulmala et al., 2009). The three other sites outside Europe are Manaus in Brazil, New Delhi in India and Beijing in China. These four sites comprise significant sources in areas with previously limited long-term aerosol measurements. At these four non-European EUCAARI measurements sites, the scientific emphasis has been placed on aerosol optical properties, indirect aerosol effects, aerosol chemistry, new particle formation and the validation of satellite and modelling results. In South Africa, one of the specific interests is to improve the interpretation of remote sensing methods, as common approaches may not be valid due to the complex layered structure of the troposphere.

**South African
EUCAARI –
measurements**

L. Laakso et al.

Title Page

Abstract

Introduction

Conclusions

References

Tables

Figures

⏪

⏩

◀

▶

Back

Close

Full Screen / Esc

Printer-friendly Version

Interactive Discussion



In this paper, the first results from EUCAARI measurements conducted in the Highveld area will be presented, along with a detailed description of the site, its regional characteristics, instrumentation and measurement procedures. The main purpose of this article is to provide a reference for future work. As part of this process, a preliminary analysis of measurement data from a short period in early June 2009 will be presented to demonstrate the high variability of pollutant concentrations and their relation to regional meteorological conditions.

2 Regional characteristics of the South African Highveld

2.1 Meteorology

The meteorological situation in South Africa is subject to a strong seasonal variability. Above Central Highveld, the atmospheric circulation pattern is dominated by anticyclonic circulation during the winter and frequent easterly disturbances during the summer. Westerly disturbances take place approximately 20% of the time throughout the year (Garstang et al., 1996). The precipitation is characterized by strong seasonal variation with practically all precipitation coming during wet season starting typically in October and ending in March. The precipitation cycle strongly affects local pollutant concentrations via primary emissions from wild fires and wet scavenging by precipitation and clouds.

The cloud cover over the Highveld is often limited due to a dominant high pressure system, created by the high altitude and the subtropical subsidence (Tyson and Preston-Whyte, 2000). This, combined with low heat capacity of the soil, creates frequent inversions that significantly reduce the vertical mixing (Garstang et al., 1996). These inversions are most pronounced just before sunrise. In the presence of sunlight the inversions begin to break down through convective heating and the height of the mixed layer is increased (Tyson et al., 1996; Tyson and Preston-Whyte, 2000).

South African EUCAARI – measurements

L. Laakso et al.

Title Page

Abstract

Introduction

Conclusions

References

Tables

Figures



Back

Close

Full Screen / Esc

Printer-friendly Version

Interactive Discussion



South African EUCAARI – measurements

L. Laakso et al.

Title Page

Abstract

Introduction

Conclusions

References

Tables

Figures

◀

▶

◀

▶

Back

Close

Full Screen / Esc

Printer-friendly Version

Interactive Discussion



These specific meteorological conditions modulate the pollutant levels above Highveld. With the high occurrence of anticyclonic circulations, pollutants can be trapped over Southern Africa for several days before exiting the sub-continent, primarily towards the east coast via a well defined plume (Garstang et al., 1996; Freiman and Piketh, 2002; Piketh et al., 2000). Example of this circulation is visible in Fig. 1, which represents the statistical distribution of HYSPLIT 96-h back trajectories (Draxler and Hess, 2004) for the years 2006–2007.

Aerosol particles, that are transported via this pathway may also be trapped below stable layers found preferentially at ~850 hPa (over coastal regions), ~700 hPa, ~500 hPa and ~300 hPa on no-rain days (Tyson and Preston-Whyte, 2000). The 500 hPa layer is most persistent and usually caps pollutants in a haze layer over Southern Africa. The layered structure is at its strongest during the winter months.

2.2 Emissions in the Highveld area

Figure 2 shows the population density estimate for 2010 for Southern Africa with a $0.25^\circ \times 0.25^\circ$ spatial resolution (CIESIN, 2010). The population density is an indicator of non-industrial human activities, as well as the propitiousness of local ecosystem for human living.

Figure 3 shows the total emissions of SO_2 based on the SAFARI 2000 emission inventory (Fleming and van der Merwe, 2004). The main point sources of pollutants in the Highveld are coal-based power stations, petrochemical industry, as well as mining and metallurgical industries. The major pollutants released by these industries include SO_2 , NO_x and particulates, whilst the petrochemical industry additionally emits VOCs, H_2S and NH_3 (Cardoso et al., 1997). During winter a significant contribution of pollutants originates from domestic burning in informal settlements (June–August) and wild fires (July–September). These emissions contain NO_x , CO, VOCs and particulate matter (PM), with the largest contribution from black carbon. In addition, windblown dust from soil and the mining industry contribute to high PM concentrations especially during the dry season.

3 The measurement site

The Elandsfontein measurement station (26°14'43" S, 29°25'30" E) is located on the top of a hill approximately 200 km east of Johannesburg (Fig. 1) (e.g. Collett et al., 2010). The average altitude of the area varies between 1400 and 1600 m above mean sea level (a.m.s.l.), while the hill top where the measurement station is situated is 1750 m a.m.s.l. The shortest distance to the Indian Ocean is approximately 350 km. The Drakensberg mountains between the ocean and the site reach heights of 2000–3500 m a.m.s.l.

The major pollution sources within a 50 km radius include six coal-fired power plants to the west and north and a petrochemical coal plant to the south-west of the monitoring station (Fig. 4). The site is also relatively frequently impacted by metallurgical plants to the north. However, there are no major pollution sources within a radius of 20 km of the site and in particular, in the sector between north-east and south east only few distant industrial plants are known (Lourens et al., 2009).

The vegetation around the site is typical dry grassland pasture and farmland (Caruthers, 1997), with annual precipitation of about 700 mm. The rain season is during the period October–March with very little rain during the winter (SAWS, 2009). The average maximum daytime temperatures in summer and winter are 26 °C and 17 °C, respectively, and the corresponding average low night temperatures are 14 °C and 1 °C.

4 Measurements and technical solutions

The instrumentation at the Elandsfontein monitoring site is housed in two small, air conditioned huts. An additional metal shelter houses the pumps and compressor, whilst a LIDAR and Partisol aerosol sampler have been placed in a separate shelter. In addition to the instrumentation, the site is equipped with tools and spare parts for routine maintenance and instrument servicing. The full aerosol measurements were started on 11 February 2009 and have been operational ever since, except for short time periods

Title Page

Abstract

Introduction

Conclusions

References

Tables

Figures

◀

▶

◀

▶

Back

Close

Full Screen / Esc

Printer-friendly Version

Interactive Discussion



when maintenance, instrument service and power failures occurred.

Summary of the instruments is shown in Table 1.

4.1 Meteorological observations

Basic meteorological parameters on the site are measured with a Vaisala WXT510 meteorological station. The observations include wind direction and speed with an acoustic anemometer, temperature, relative humidity, and rain intensity (Vaisala, WTX510 specification sheet, 2010). In addition to the weather station observations, solar radiation is measured with a PAR sensor and the potential temperature gradient with two Rotronic T-RH sensors stationed at heights of 2 and 8 m.

4.2 Trace gas observations

The trace gases are measured as a part of ESKOM's routine air quality monitoring.

SO₂, NO_x and O₃ are measured with a Thermo Electron 43C SO₂ analyser, a Thermo Electron 42i NO_x analyser and a Monitor Europe ML9810B O₃ analyser, respectively. H₂S is measured with a Thermo Electron 43A SO₂ analyzer with a Thermo Electron 43A converter.

4.3 Aerosol observations

In order to avoid changes in aerosol properties due to humidity variations, all aerosol instruments are connected to an inlet drier (Tuch et al., 2009). The aerosol sample flow is kept below 35% relative humidity to avoid hygroscopic growth of particles, condensation and potential sparking inside the instruments. Particles larger than 10 μm in aerodynamic diameter were excluded using a PM₁₀ inlet. Inside the measurement hut, the incoming air flow is split between the different instruments.

South African EUCAARI – measurements

L. Laakso et al.

Title Page

Abstract

Introduction

Conclusions

References

Tables

Figures

◀

▶

◀

▶

Back

Close

Full Screen / Esc

Printer-friendly Version

Interactive Discussion



4.3.1 Number size distributions

A non-commercial Scanning Mobility Particle Sizer (SMPS) built by Leibniz Institute for Tropospheric Research (IfT), Leipzig, Germany, is used. It consists of a differential mobility particle analyzer with a closed loop arrangement and a TSI 3010 condensation particle counter. The instrument measures particles between 10 nm and 870 nm diameter with a 5-min time resolution.

An optical particle counter (OPC, Grimm Model 1.108) was used in May through September for measuring the particle number size distribution in the diameter range 0.3–20 μm . The flow rate of the OPC was 1.2 L per minute (LPM). The particle number size distributions obtained from the OPC were combined with those measured with the SMPS to cover the diameter range of 10 nm to 20 μm . The merging of the data was done by comparing the data on overlapping size range and scaling the OPC-concentrations to SMPS data.

In September 2009, the OPC was temporarily replaced with a Grimm model 7.66 OPC with a maximum particle diameter of 2.2 μm . In order to cover the missing range between 2.2 μm and 10 μm , an additional OPC based on the optics of a DMT-CCNC counter with a measurement range of 0.7–10 μm was installed in September 2009.

4.3.2 Aerosol light absorption measurements

Light absorption by particles is measured with two different instruments: a Multi-Angle Absorption Photometer (MAAP) (Petzold and Schönlinner, 2004) at $\lambda=637$ nm and a 3-wavelength Particle Soot Absorption Photometer (PSAP) (Virkkula et al., 2005) at $\lambda=467$, 530, and 660 nm. The PSAP is a filter-based method with a manual filter change. In principle, this might have created problems since the station was visited only once every 12 days. In order to prolong the filter changing period, the sample flow is diluted at the ratio of approximately 1:10. A detailed description of the performance of this system will be presented in a separate paper.

Title Page

Abstract

Introduction

Conclusions

References

Tables

Figures

◀

▶

◀

▶

Back

Close

Full Screen / Esc

Printer-friendly Version

Interactive Discussion



4.3.3 Aerosol light scattering measurements

Light scattering was measured at three wavelengths (450, 520, and 700 nm) by an Ecotech Aurora 3000 integrating nephelometer. This commercial instrument was modified with a new light source and an inlet flow control system for automatic span checks.

5 The zero and span of the instrument were automatically checked every day at midnight with a particle filter and high grade CO₂.

4.3.4 Solar irradiance and aerosol optical depth measurements

The solar irradiance and sky radiance was measured with a Cimel multichannel Sun-photometer. The Sunphotometer at Elandsfontein is part of the global AERONET ob-
10 servation network (<http://aeronet.gsfc.nasa.gov/index.html>) (Holben et al., 1998).

4.3.5 Aerosol sampling and analysis of chemical composition

In addition to the in situ measurements, aerosol particles were collected for chemical analysis at a flow rate of 1 m³ h⁻¹ (at ambient conditions) on 47 mm quartz filters using a dichotomous aerosol sampler (2025 Partisol) equipped with a PM₁₀ inlet. Quartz and
15 paper filters were not pre-treated prior to analysis. Fine particles (aerodynamic diameter below 2.5 μm) and coarse particles (aerodynamic diameter between 2.5 and 10 μm) were collected simultaneously every 6 days for a collection period of 24 h starting from 08:00 a.m. These measurements were finished in January 2010.

To avoid negative sampling artefacts, due to volatilization of ammonium nitrate from the quartz substrates, a Whatman 41 paper filter was sampled on the back of each quartz filter and the concentration of ammonium and nitrate were calculated as the sum of quartz and paper concentrations (Gilardoni et al., 2010).

Denuder units were employed to avoid positive sampling artefacts due to absorption of gas species on the sampling substrate. Volatile organic carbon compounds were
25 removed upstream of the filters with an activated carbon honeycomb denuder, while

Title Page

Abstract

Introduction

Conclusions

References

Tables

Figures

⏪

⏩

◀

▶

Back

Close

Full Screen / Esc

Printer-friendly Version

Interactive Discussion



nitric acid and ammonia were removed with glass denuders coated by sodium chloride and citric acid, respectively.

Concentrations of fine and coarse mass were determined by gravimetric analysis. Organic carbon (OC) and elemental carbon (EC) were measured by thermo-optical analysis with a Sunset Laboratory Dual-Optical analyzer (Birch and Cary, 1996); a modified version of the protocol EUSAAR-2 was employed (Cavalli et al., 2010) with a longer heating step to guarantee the complete evolution of carbonaceous aerosol fractions. Concentrations of the major inorganic ions (Na^+ , NH_4^+ , K^+ , Mg^{2+} , Ca^{2+} , Cl^- , NO_3^- , PO_4^{3-} , SO_4^{2-}) were determined by ion chromatography (IC) after filter extraction with ultra pure water (Putaud et al., 2002).

Soil compounds were sampled on polycarbonate filters for a few weeks each season to determine the unidentified fractions of the samples. Field blanks for comparisons were collected monthly.

All the chemical analyses were carried out by European Union Research centre JRC-Ispra.

4.3.6 Vertical aerosol back scattering profiles

A portable aerosol Raman LIDAR system extended PollyXT was developed at the IfT, Germany (Althausen et al., 2009). Its development ties up to the demand for a Raman LIDAR systems requiring less effort concerning operating personnel, logistics and power consumption, while utilizing the latest developments in systems parts. The system is a 3+2 Raman LIDAR with a depolarization channel. The instrument is completely remotely controlled and all measurements are performed automatically. For aviation safety purposes, the system is equipped with an airplane detecting radar which shuts down the laser beam when detecting an aircraft. The Lidar was installed at the site in December 2009 and the measurements are scheduled to continue until January 2011.

South African EUCAARI – measurements

L. Laakso et al.

Title Page

Abstract

Introduction

Conclusions

References

Tables

Figures

⏪

⏩

◀

▶

Back

Close

Full Screen / Esc

Printer-friendly Version

Interactive Discussion



4.4 Data logging systems

Due to the fairly large number of instruments, the data logging system is based on a network of three PC's plus a separate PC for the Lidar. One of the three PCs is used to run the SMPS system, another to control the sample dryer and to log data from the Nephelometer. All the other instruments except the LIDAR are connected to the third "Master" PC that uses a 3G modem to send the measurement and diagnostics data to a server in Helsinki once a day. The data transmission from the LIDAR is operated via a separate 3G modem.

The data from the Nephelometer, MAAP, OPC and the weather station are collected via serial port connections. Analog signals for gases, temperature profile, solar radiation and instrument flow rates are collected with Pico ADC-16 (Pico Technology Ltd.) loggers.

4.5 Power and signal protection

Due to the location of the site on the top of a hill, unreliable electricity supply and severe lightning were of major concern. The power and logging system are therefore equipped with a multi-step power protection system. First, the incoming power line is equipped with a ground breaker that reduces the incoming voltages in the event of a lightning surge on the incoming power line. Next, the incoming power is divided into three 3-phase groups. Each group has its own independent three-phase under- and over-voltage relay set at 210 and 240 V, respectively. The relays have 1 to 3-min time delays after a break to protect the instrumentation from repetitive short-lived irregularities in the power supply. The time delays of each group are set differently to ramp up the electrical load more evenly after a power failure. Each group also has a residual current switch. For additional protection, the sensitive measurement instruments and computers are connected to an UPS. The grounding of the measurement huts are connected to the grounding net of a 70 m high microwave link mast at the site. The mast provides additional protection for the entire measurement site.

Title Page

Abstract

Introduction

Conclusions

References

Tables

Figures

◀

▶

◀

▶

Back

Close

Full Screen / Esc

Printer-friendly Version

Interactive Discussion



In addition to protection against electrical disturbances, the measurement huts are equipped with temperature controllers to stop the measurements in case of high temperatures, e.g. malfunctioning air conditioner.

The signals from sensors outside the huts are optically isolated from the measurement computers. The serial port communication to the weather station, gas analysers, and solar radiation data loggers were isolated via optical fibre. These Pico-loggers are also protected with varistors against high voltages in the analogue signals.

5 Site maintenance and data-analysis methods

5.1 Instrument maintenance and servicing

The site is visited at least once every 12 days for calibrations, instrument servicing and routine maintenance. During the visits, all instruments and data logging are checked. Next, a HEPA particle filter is placed on the common aerosol inlet, to verify that all the particle instruments show zero concentrations. After this common inlet check, the zero of the SMPS is checked separately for leaks inside the instrument. The nephelometer automatic zero and span for the previous day is checked and if the values are out of range, full calibration and adjustment is performed. Due to potential variation of the CO₂ span calibration, the span of the nephelometer is checked every two months with external high grade CO₂. The flows of all inlets and sheath air are measured and recorded. If the flows are out of range, they are adjusted. The PM₁₀ inlets are cleaned and greased with silicon grease. The filters of the Partisol sampler are changed and the status values recorded. The gas analyzers are calibrated once a month and adjusted when needed.

A full maintenance service of the site is carried out approximately every three months. This includes more complicated service procedures such as the SMPS service, measurement instrumentation cell cleaning and other necessary servicing procedures.

Title Page

Abstract

Introduction

Conclusions

References

Tables

Figures

⏪

⏩

◀

▶

Back

Close

Full Screen / Esc

Printer-friendly Version

Interactive Discussion



In addition to on-site checks, the data downloaded to the server is visually inspected a few times per week for quality assurance. If irregularities are found, extra site visits and necessary actions are carried out.

5.2 Data processing

5 The measurement data from the site is visualized and corrected with a fit-for-purpose Matlab program set, which corrects the data for span and zero calibrations, instrument errors, and flow checks. Quality of SMPS data is investigated during the data inversion.

6 Results

10 A comprehensive data analysis of the entire measurement period is scheduled for late-2010. In this paper results obtained for a 9-day period (2–10 June 2009) are presented to indicate some of the extreme cases typical for the measurement site during the early winter period. The time resolution of data series shown here are 1-min for meteorological variables, except 5 min for SMPS and OPC and 1-h for trace gases and aerosol optical properties.

15 6.1 Meteorological data

The time series of basic meteorological variables during the 9-day period considered here is shown in Figs. 5 and 6. During the first few days, daily temperature variations were $\sim 10^{\circ}\text{C}$ and the relative humidity was mostly below 30%. The decrease in pressure on 6 June was followed by an obvious diurnal temperature change and a strong
20 increase in the relative humidity on the evening of 7 June, indicating a change in synoptic weather conditions. The change in weather was reflected in the solar radiation intensity and the value of the potential temperature gradient reflecting the surface inversion. The first four days of the period (2–5 June) were sunny, whereas 6, 7 and 9

South African EUCAARI – measurements

L. Laakso et al.

Title Page

Abstract

Introduction

Conclusions

References

Tables

Figures

◀

▶

◀

▶

Back

Close

Full Screen / Esc

Printer-friendly Version

Interactive Discussion



June were partly cloudy and both 8 and 10 June cloudy. It was also apparent that the cloudy days had smaller potential temperature gradients than the other days.

6.2 Trace gases

Figure 7 presents the trace gas concentrations between 1 and 2 June. The measured ozone concentrations depended strongly on the weather conditions. During this period, air masses coming from the north-westerly sector had O₃ concentrations as high as 100 ppb, whereas during the easterly winds the concentrations dropped down to about 40 ppb. The concentrations of SO₂, NO_x and H₂S were variable with, in the period 2–6 June, some clear peaks in the morning and afternoon; the similarity in these patterns suggest a similar source, i.e. industrial plumes from a westerly sector is quite evident. On 5 June, the SO₂, NO_x and H₂S concentrations peaked at exactly the same time as a decrease in the O₃ concentrations was observed. This kind of behaviour is typical in fresh plumes from major NO emitting sources (e.g. Sillman, 1999). During days with westerly winds, SO₂-concentrations can have instantaneous peaks above 100 ppb, which is indicative of very strong regional point sources. During days with winds from the eastern sector gaseous pollutant concentrations were close to low regional background values (Martins et al., 2009). Obviously concentrations were also reduced by wet scavenging during 8–10 June.

6.3 Aerosol physical properties

The merged SMPS and OPC size distribution data are shown in Fig. 8 together with the total number and PM₁₀ concentrations. The data in Fig. 8 shows that atmospheric new particle formation took place on every sunny day between 2 and 7 June, with particle number concentrations frequently exceeding the value of 10 000 cm⁻³. The highest particle number concentration was observed during the early night between 4 and 5 June. The reason for this peak in concentration was primary emission rather than atmospheric new particle formation, as the peak was associated with relatively

Title Page

Abstract

Introduction

Conclusions

References

Tables

Figures

◀

▶

◀

▶

Back

Close

Full Screen / Esc

Printer-friendly Version

Interactive Discussion



high mean particle size (Fig. 8) and high levels of absorbing aerosols (Fig. 9). The cloudy period of 8–10 June with easterly winds showed very low particle number concentrations with minima of about 100 cm^{-3} , e.g. during the night of 9–10 June. The low particle concentrations during the night of 9–10 June can be explained by aerosol-cloud interactions when warm and humid air masses from the Indian Ocean passed over the Drakensberg mountains before passing over the site. The two rain events on 10 June had stronger effects on the particle mass concentrations than particle number concentrations as the large particle wash out easier than particles of Aitken and accumulation sizes.

The scattering coefficients were first corrected for pressure and temperature so that the data discussed below are at 1013 mbar and 273 K, as are the absorption coefficients. The scattering coefficients were interpolated logarithmically to the MAAP wavelength 637 nm in order to calculate single-scattering albedo (SSA).

The aerosol scattering and absorption coefficients followed each other closely during the measurement period (Fig. 9). During westerly winds (2–7 June) when high particle mass concentrations were encountered, the aerosol scattering coefficient was frequently in the range $100\text{--}300 \text{ M m}^{-1}$. Such high values are rare, even in urban or other polluted environments (Cabada et al., 2004; Chand et al., 2006; Lymani et al., 2008), although in China even higher scattering coefficients are observed (e.g., Bergin et al., 1999; Andreae et al., 2008; Garland et al., 2009). During 8–10 June when relatively clean easterly air masses prevailed, the aerosol scattering coefficient showed values typical for remote environments (Delene et al., 2002; Aaltonen et al., 2006). The value of the single scattering albedo (SSA) was most of the time between 0.8 and 0.9 regardless of the level of pollution, which is comparable to the value of 0.85 ± 0.02 obtained for a biomass burning aerosol during the SAFARI 2000 field campaign over Southern Africa (Leahy et al., 2007). The reason for the occasional, very low values of SSA associated with high black carbon concentrations remain unclear, since they did not co-occur with major changes in measured trace gas concentration or meteorological quantities (see also Fig. 11c).

**South African
EUCAARI –
measurements**

L. Laakso et al.

Title Page

Abstract

Introduction

Conclusions

References

Tables

Figures

◀

▶

◀

▶

Back

Close

Full Screen / Esc

Printer-friendly Version

Interactive Discussion



**South African
EUCAARI –
measurements**

L. Laakso et al.

[Title Page](#)[Abstract](#)[Introduction](#)[Conclusions](#)[References](#)[Tables](#)[Figures](#)[⏪](#)[⏩](#)[◀](#)[▶](#)[Back](#)[Close](#)[Full Screen / Esc](#)[Printer-friendly Version](#)[Interactive Discussion](#)

The scattering coefficients at 450, 520, and 700 nm were used to calculate Ångström exponent (\AA) of scattering. It is commonly used as a qualitative indicator of aerosol particle size, with large values (>2) indicating the dominance of small particles, and small values (<1) the dominance of large particles, even though it has been shown that for multimodal size distributions even this is not necessarily true (e.g., Schuster et al., 2006). In the present paper a more detailed analysis of this is omitted, however, just some qualitative observations are presented.

\AA was close to 2 during the polluted conditions (3–7 June), which indicates a clear dominance of submicron particles over supermicron particles in measured air masses (see also Fig. 8) After this period (8–10 June), the value of \AA fluctuated more, which suggests that supermicron particles occasionally contributed to the total aerosol particle population (see also Fig. 11d).

6.4 Aerosol chemical composition

The aerosol chemical composition was analyzed for two 24-h periods, starting at 08:00 a.m. on 2 June and 8 June. The mass concentrations of fine and coarse particles were 43.3 and $50.4 \mu\text{g m}^{-3}$ on 2 June and 3.7 and $8.3 \mu\text{g m}^{-3}$ on 8 June, respectively. The major constituents of the aerosol were organic and elemental carbon (OC and EC) and inorganic ions. The concentration of organic matter (OM) was calculated from the OC concentrations assuming OM to OC ratio equal to 1.8 and 2.4. The OM to OC ratio reported in literature varies between 1.4, for fresh aerosol, to 2.4 and higher for more oxidized and aged aerosol (Russell et al., 2003). Downwind of urban areas this ratio varied between 1.8 and 2.4 (Gilardoni et al., 2009). Since no OM/OC values were available for Elandsfontein, the OM concentration was calculated using both the lower and upper bounds of the interval reported by Gilardoni et al. (2009); the corresponding reconstructed fine mass was 78% and 90% of the gravimetric mass.

During the two days the contribution of OM, sulfate, and ammonium to fine mass was similar: 37–32% (50–43%), 19–16%, and 8–6%, respectively. On 2 June the percentage of nitrate was 10%, while it was less than 1% on 8 June; similarly, EC

concentration sharply decreased from 4% to less than 1%. The largest contribution of nitrate and EC overlapped with the peaks of NO and NO₂ and the high concentration of BC on 2 June. The relative larger contribution of sodium, potassium, and chloride on 8 June compared with 2 June might indicate the transport of sea-salt aerosol from the Indian Ocean to the measurement site. The differences in fine aerosol composition highlight the influence of industrial sources on 2 June and the influence of cleaner (possible marine) air masses on 8 June.

The reconstructed chemical coarse mass was less than 20% of the gravimetric mass, likely due to a significant contribution of dust, not monitored during the first part of the sampling campaign. Future analysis will be carried out to characterize the remaining mass percentage and to determine the contribution of mineral dust to the aerosol loading.

6.5 Relationships between measured aerosol properties

The previous sections demonstrated the very high temporal variability of pollutant concentrations associated with the transport of different air mass types to the measurement site. As a matter of fact, the particle mass and number concentrations and the aerosol scattering and absorption coefficients varied by more than two orders of magnitude during the 9-day measurement period considered here. In this section the connection between the measured aerosol properties during the same time period will be considered. The data will be presented in four different ways: i) data covering the whole period, ii) data measured during a new-particle formation event day on 3 June, iii) data measured during a clean period on 9 June, and iv) data measured during a rainy period on 10 June.

Of the measured aerosol properties, the highest correlation (0.89) was found between the aerosol scattering and absorption coefficient (Fig. 10). The connection between these two quantities was strongest during the polluted conditions when the scattering coefficient was mostly above 10 M m⁻¹. Atmospheric new particle formation did not perturb this connection, which is clear because the freshly-nucleated particles are

Title Page

Abstract

Introduction

Conclusions

References

Tables

Figures

◀

▶

◀

▶

Back

Close

Full Screen / Esc

Printer-friendly Version

Interactive Discussion



too small to scatter light significantly. Even after the new particle formation events SSA remained at ~ 0.8 suggesting that particles emitted from primary sources, such as soot from combustion and then coated with sulphates and organics determined the aerosol optical properties in polluted air masses.

Figure 11a–d shows the relationship between the aerosol mass concentration (PM_{10}) and aerosol scattering, absorption, single-scattering albedo and Ångström exponent during the measurement period. When PM_{10} concentrations were high ($>30\text{--}50\ \mu\text{g}/\text{m}^3$), aerosol scattering and absorption coefficients also peaked with correlation coefficients above 0.6. This kind of behaviour is expected due to the significant influence of pollution in the Highveld industrial area. The processes affecting the single scattering albedo and Ångström exponent were discussed previously.

The connection between PM_{10} and total particle number concentration (Fig. 12a) was more complicated, mainly due to atmospheric new particle formation causing large variations in total particle number concentrations and size distributions under polluted conditions. Figure 12b suggests that there is a trend between PM_{10} and SO_2 , although for mass concentrations less than $20\ \mu\text{g}/\text{m}^3$ and SO_2 -concentrations less than 4 ppb there seems to be no correlation. This is no surprise since SO_2 has an anthropogenic source as do the larger particles that govern PM_{10} concentrations. Figure 12c,d shows the relation between the total particle number, and aerosol scattering and absorption. It is evident that the nucleation resulting in high number concentrations does not significantly affect the optical properties. In the case of low particle number, correlation is stronger as the average particle size is larger (see also Fig. 11d). The main aerosol parameters are summarized in Table 2.

7 Conclusions

Most of the long-term aerosol measurements have been carried out in the Northern Hemisphere. In the Southern Hemisphere these measurements are sparse. Due to the limited number of measurements, aerosol processes affecting the direct and indirect

Title Page

Abstract

Introduction

Conclusions

References

Tables

Figures

⏪

⏩

◀

▶

Back

Close

Full Screen / Esc

Printer-friendly Version

Interactive Discussion



radiative forcing and precipitation properties are less understood. This hampers the evaluation of climate scenarios and development of climate change mitigation plans.

In this article initial results are presented from measurements at the South African EUCAARI experimental site. Site characteristics, instrumentation utilized, as well as the service and maintenance procedures are described. Based on data gathered over a 9-day measurement period, the following conclusions can be drawn: i) the degree of particulate and gaseous pollution reaching the site shows a high temporal variability, with the largest concentrations associated with air masses originating from the heavily-polluted industrial area of the Highveld, ii) under polluted conditions, a close connection between the particle mass concentration and aerosol scattering and absorption coefficient is usually observed, iii) under clean conditions, multiple smaller sources contribute to the atmospheric particle population, iv) aerosol optical properties are determined almost entirely by submicron primary particles during polluted conditions, whereas under clean conditions also supermicron particles may contribute, v) atmospheric new particle formation, whilst having practically no effect on aerosol mass concentration or optical properties in polluted air masses, substantially enhance particle number concentrations, even in the case of a polluted air mass.

Acknowledgement. This work is funded by the European Integrated project on Aerosol Cloud Climate and Air Quality Interactions, Academy of Finland and Vilho, Yrjö and Kalle Väisälä foundation.

References

- Aaltonen, V., Lihavainen, H., Kerminen, V.-M., Komppula, M., Hatakka, J., Eneroth, K., Kulmala, M., and Viisanen, Y.: Measurements of optical properties of atmospheric aerosols in Northern Finland, *Atmos. Chem. Phys.*, 6, 1155–1164, doi:10.5194/acp-6-1155-2006, 2006.
- Althausen, D., Engelmann, R., Baars, H., Heese, B., Ansmann, A., Müller, D., and Komppula, M.: Portable Raman lidar PollyXT for automated profiling of aerosol backscatter, extinction, and depolarization, *J. Atmos. Oceanic Technol.*, 26, 2366–2378, doi:10.1175/2009JTECHA1304.1, 2009.

South African EUCAARI – measurements

L. Laakso et al.

Title Page

Abstract

Introduction

Conclusions

References

Tables

Figures

◀

▶

◀

▶

Back

Close

Full Screen / Esc

Printer-friendly Version

Interactive Discussion



South African EUCAARI – measurements

L. Laakso et al.

Title Page

Abstract

Introduction

Conclusions

References

Tables

Figures

◀

▶

◀

▶

Back

Close

Full Screen / Esc

Printer-friendly Version

Interactive Discussion



Andreae, M. O., Schmid, O., Yang, H., Chand, D., Yu, J. Z., Zeng, L.-M., and Zhang, Y.-H.: Optical properties and chemical composition of the atmospheric aerosol in urban Guangzhou, China, *Atmos. Environ.*, 42, 6335–6350, 2008.

Bergin, M. H., Cass, G. R., Xu, J., Fang, C., Zeng, L. M., Yu, T., Salmon, L. G., Kiang, C. S., Tang, X. Y., Zhang, Y. H., and Chameides, W. L.: Aerosol radiative, physical, and chemical properties in Beijing during June 1999, *J. Geophys. Res.*, 106, D16, 17969–17980, 2001.

Birch, M. E. and Cary, R. A.: *Aerosol Sci. Technol.*, 25, 221–241, 1996.

Cardoso, A. A., Liu, H., Dasgupta, P. K.: Fluorometric fiber optic drop sensor for atmospheric hydrogen sulphide, *Talanta*, 44, 1099–1106, 1997.

Carruthers, V.: *Wildlife of Southern Africa*, Struik Publishers, Cape Town, 1997.

Cavalli, F., Viana, M., Yttri, K. E., Genberg, J., and Putaud, J.-P.: Toward a standardised thermal-optical protocol for measuring atmospheric organic and elemental carbon: the EU-SAAR protocol, *Atmos. Meas. Tech.*, 3, 79–89, doi:10.5194/amt-3-79-2010, 2010.

Cabada, J. C., Khlystov, A., Wittig, A. E., Pilinis, C., and Pandis, S. N.: Light scattering by fine particles during the Pittsburg air quality study: measurements and modelling, *J. Geophys. Res.*, 109, D16S03, doi:10.1029/2003JD004155, 2004.

Center for International Earth Science Information Network (CIESIN), Columbia University; United Nations Food and Agriculture Programme (FAO); and Centro Internacional de Agricultura Tropical (CIAT) 2005, *Gridded Population of the World: Future Estimates (GPWFE)*, Palisades, NY, Socioeconomic Data and Applications Center (SEDAC), Columbia University, available online at: <http://sedac.ciesin.columbia.edu/gpw/documentation.jsp>, access date: 10 January 2010.

Chand, D., Guyon, P., Artaxo, P., Schmid, O., Frank, G. P., Rizzo, L. V., Mayol-Bracero, O. L., Gatti, L. V., and Andreae, M. O.: Optical and physical properties of aerosols in the boundary layer and free troposphere over the Amazon Basin during the biomass burning season, *Atmos. Chem. Phys.*, 6, 2911–2925, doi:10.5194/acp-6-2911-2006, 2006.

Collett, K. S., Piketh, S. J., and Ross, K. E.: An assessment of the atmospheric nitrogen budget on the South African Highveld, *South Afr. J. Sci.*, 106, 220, doi:10.4102/sajs.v106i5/6.220, 2010.

Delene, D. J. and Ogren, J. A.: Variability of aerosol optical properties at four North American surface monitoring sites, *J. Atmos. Sci.*, 59, 1135–1150, 2002.

Draxler R. R. and Hess, G. D.: *Description of the HYSPLIT_4 Modeling System*, NOAA Technical Memorandum ERL ARL-224, NOAA, Maryland, USA, 2004.

South African EUCAARI – measurements

L. Laakso et al.

Title Page

Abstract

Introduction

Conclusions

References

Tables

Figures

◀

▶

◀

▶

Back

Close

Full Screen / Esc

Printer-friendly Version

Interactive Discussion



Fleming, G. and van der Merwe, M.: Spatial disaggregation of greenhouse gas emission inventory data for Africa South of the equator, available at: <http://gis.esri.com/library/userconf/proc00/professional/papers/PAP896/p896.htm>, 2004, access date: 1 April 2010.

Forster, P., Ramaswamy, V., Artaxo, P., Bernsten, T., Betts, R., Fahey, D. W., Haywood, J., Lean, J., Lowe, D. C., Myhre, G., Nganga, J., Prinn, R., Raga, G., Schulz, M., and Van Dorland, R.: Changes in atmospheric constituents and in radiative forcing, in: *Climate Change 2007: The Physical Science Basis. Contribution of Working Group I to the Fourth Assessment Report of the Intergovernmental Panel on Climate Change*, edited by: Solomon, S., Qin, D., Manning, M., Chen, Z., Marquis, M., Averyt, K. B., Tignor, M., and Miller, H. L., Cambridge University Press, Cambridge, UK and New York, NY, USA, 2007.

Freiman, M. T. and Piketh, S. J.: Air transport into and out of the industrial Highveld region of South Africa, *J. Appl. Meteorol.*, 42, 994–1002, 2002.

Garland, R. M., Schmid, O., Nowak, A., Achtert, P., Wiedensohler, A., Gunthe, S. S., Takegawa, N., Kita, K., Kondo, Y., Hu, M., Shao, M., Zeng, L. M., Zhu, T., Andreae, M. O., and Pöschl, U.: Aerosol optical properties observed during Campaign of Air Quality Research in Beijing 2006 (CAREBeijing-2006): characteristic differences between the inflow and outflow of Beijing city air, *J. Geophys. Res.*, 114, D00G04, doi:10.1029/2008JD010780, 2009.

Garstang, M., Tyson, M., Swap, R., Edwards, M., Kållberg, P., and Lindesay, J. A.: Horizontal and vertical transport of air over Southern Africa, *J. Geophys. Res.*, 101, 23721–23736, 1996.

Gilardoni, S., Liu, S., Takahama, S., Russell, L. M., Allan, J. D., Steinbrecher, R., Jimenez, J. L., De Carlo, P. F., Dunlea, E. J., and Baumgardner, D.: Characterization of organic ambient aerosol during MIRAGE 2006 on three platforms, *Atmos. Chem. Phys.*, 9, 5417–5432, doi:10.5194/acp-9-5417-2009, 2009.

Gilardoni, S., Vignati, E., Marmer, E., Cavalli, F., Belis, C., Gianelle, V., Loureiro, A., and Artaxo, P.: Sources of carbonaceous aerosol in the Amazon Basin, *Atmos. Chem. Phys. Discuss.*, 10, 29923–29969, doi:10.5194/acpd-10-29923-2010, 2010.

Hansen, J., Sato, M., Ruedy, R., Kharecha, P., Lacis, A., Miller, R. L., Nazarenko, L., Lo, K., Schmidt, G. A., Russell, G., Aleinov, I., Bauer, S., Baum, E., Cairns, B., Canuto, V., Chandler, M., Cheng, Y., Cohen, A., Del Genio, A., Faluvegi, G., Fleming, E., Friend, A., Hall, T., Jackman, C., Jonas, J., Kelley, M., Kiang, N. Y., Koch, D., Labow, G., Lerner, J., Menon, S., Novakov, T., Oinas, V., Perlwitz, J., Perlwitz, J., Rind, D., Romanou, A., Schmunk, R., Shindell, D., Stone, P., Sun, S., Streets, D., Tausnev, N., Thresher, D., Unger, N., Yao, M.,

South African EUCAARI – measurements

L. Laakso et al.

Title Page

Abstract

Introduction

Conclusions

References

Tables

Figures

◀

▶

◀

▶

Back

Close

Full Screen / Esc

Printer-friendly Version

Interactive Discussion



and Zhang, S.: Climate simulations for 1880–2003 with GISS modelE, *Clim. Dynam.*, 29, 661–696, 2007.

Held, G., Scheifinger, H., Snyman, G. M., Tosen, G. R., and Zunckel, M.: The Climatology and Meteorology of the Highveld, in: *Air pollution and its impacts on the South African Highveld*, edited by: Held, G., Gore, B. J., SurrIDGE, A. D., Tosen, G. R., Turner, C. R., and Walmsey, R. D., Environmental Scientific Association Cleveland, 1996.

Holben B. N., Eck, T. F., Slutsker, I., Tanre, D., Buis, J. P., Setzer, A., Vermote, E., Reagan, J. A., Kaufman, Y., Nakajima, T., Lavenu, F., Jankowiak, I., and Smirnov, A.: AERONET – a federated instrument network and data archive for aerosol characterization, *Remote Sens. Environ.*, 66, 1–16, 1998

Jayarathne, E. R. and Verma, T. S.: The impact of biomass burning on the environmental aerosol concentration in Gaborone, Botswana, *Atmos. Environ.*, 35, 1821–1828, 2001.

Kulmala, M., Asmi, A., Lappalainen, H. K., Carslaw, K. S., Pöschl, U., Baltensperger, U., Hov, Ø., Brenquier, J.-L., Pandis, S. N., Facchini, M. C., Hansson, H.-C., Wiedensohler, A., and O'Dowd, C. D.: Introduction: European Integrated Project on Aerosol Cloud Climate and Air Quality interactions (EUCAARI) – integrating aerosol research from nano to global scales, *Atmos. Chem. Phys.*, 9, 2825–2841, doi:10.5194/acp-9-2825-2009, 2009.

Laakso, L., Koponen, I. K., Mönkkönen, P., Kulmala, M., Kerminen, V.-M., Wehner, B., Wiedensohler, A., Wu, Z., Hu, M.: Aerosol particles in the developing world; a comparison between New Delhi in India and Beijing in China, *Water Air Soil Poll.*, 1–16, 5–20, doi:10.1007/s11270-005-9018-5, 2006.

Laakso, L., Laakso, H., Aalto, P. P., Keronen, P., Petäjä, T., Nieminen, T., Pohja, T., Siivola, E., Kulmala, M., Kgabi, N., Molefe, M., Mabaso, D., Phalatse, D., Pienaar, K., and Kerminen, V.-M.: Basic characteristics of atmospheric particles, trace gases and meteorology in a relatively clean Southern African Savannah environment, *Atmos. Chem. Phys.*, 8, 4823–4839, doi:10.5194/acp-8-4823-2008, 2008.

Leahy, L. V., Anderson, T. L., Eck, T. F., and Bergstrom, R. W.: A synthesis of single scattering albedo of biomass burning aerosol over Southern Africa during SAFARI 2000, *Geophys. Res. Lett.*, 34, L12814, doi:10.1029/2007GL029697, 2007.

Lourens, S.: VOC's on Highveld, MSc-thesis, North-West University, Republic of South Africa, 2009,

Lyamani, H., Olmo, F. J., and Alodo-Arboleda, L.: Light scattering and absorption properties of aerosol particles in the urban environment of Granada, Spain, *Atmos. Environ.*, 42, 2630–

2642, 2008.

MAAP: Available at: <http://www.thermo.com/com/cda/product/detail/0,1055,19884,00.html>, access date: 1 April 2010.

Martins, J. J., Dhammapala, R. S., Lachmann, G., Galy-Lacaux, C., Pienaar, J. J.: Long-term measurements of sulphur dioxide, nitrogen dioxide, ammonia, nitric acid and ozone in Southern Africa using passive samplers, *South Afr. J. Sci.*, 103, 336–342, 2007.

Petzold, A. and Schönlinner, M.: Multi-angle absorption photometry – a new method for the measurement of aerosol light absorption and atmospheric black carbon, *J. Aerosol Sci.*, 35, 421–441, 2004.

Piketh, S., Tyson, P., and Steffen, W.: Aeolian transport from Southern Africa and iron fertilization of marine biota in the South Indian Ocean, *South Afr. J. Sci.*, 96, 244–246, 2000.

Putaud, J.-P., Van Dingenen, R., and Raes, F.: Submicron aerosol mass balance at urban and semirural sites in the Milan area (Italy), *J. Geophys. Res.*, 107, 8198, 2002.

Rissler, J., Vestin, A., Swietlicki, E., Fisch, G., Zhou, J., Artaxo, P., and Andreae, M. O.: Size distribution and hygroscopic properties of aerosol particles from dry-season biomass burning in Amazonia, *Atmos. Chem. Phys.*, 6, 471–491, doi:10.5194/acp-6-471-2006, 2006.

Ross, K. E., Piketh, S. J., Bruintjes, R. T., Burger, R. P., Swap, R. J., and Annegarn, H. J.: Spatial and seasonal variations in CCN distribution and the aerosol-CCN relationship over Southern Africa, *J. Geophys. Res.*, 108, 8481, doi:10.1029/2002JD002384, 2003

Russell, L. M.: Aerosol organic-mass-to-organic-carbon ratio measurements, *Environ. Sci. Technol.*, 37, 2982–2987, 2003.

SAWS: Available at: <http://www.weathersa.co.za/Climat/Climstats/BethalStats.jsp>, access date: 1 April 2010.

Schuster, G. L., Dubovik, O., and Holben, B. N.: Angstrom exponent and bimodal aerosol size distributions, *J. Geophys. Res.*, 111, D07207, doi:10.1029/2005JD006328, 2006.

Sillman, S.: The relation between ozone, NO_x and hydrocarbons in urban and polluted rural environments, *Atmos. Environ.*, 33, 1821–1845, 1999.

Suni, T., Kulmala, M., Hirsikko, A., Bergman, T., Laakso, L., Aalto, P. P., Leuning, R., Cleugh, H., Zegelin, S., Hughes, D., van Gorsel, E., Kitchen, M., Vana, M., Hörrak, U., Mirme, S., Mirme, A., Sevanto, S., Twining, J., and Tardos, C.: Formation and characteristics of ions and charged aerosol particles in a native Australian Eucalypt forest, *Atmos. Chem. Phys.*, 8, 129–139, doi:10.5194/acp-8-129-2008, 2008.

Swap, R. J., Annegarn, H. J., Suttles, J. T., King, M. D., Platnick, S., Privette, J. L., and

**South African
EUCAARI –
measurements**

L. Laakso et al.

Title Page

Abstract

Introduction

Conclusions

References

Tables

Figures

◀

▶

◀

▶

Back

Close

Full Screen / Esc

Printer-friendly Version

Interactive Discussion



South African EUCAARI – measurements

L. Laakso et al.

Title Page

Abstract

Introduction

Conclusions

References

Tables

Figures

◀

▶

◀

▶

Back

Close

Full Screen / Esc

Printer-friendly Version

Interactive Discussion



- Scholes, R. J.: Africa burning: a thematic analysis of the Southern African regional science initiative (SAFARI 2000), *J. Geophys. Res.*, 108, 8465, doi:10.1029/2003JD003747, 2003.
- Tyson, P. D., Garstang, M., and Swap, R.: Large-scale recirculation of Air over Southern Africa, *J. Appl. Meteorol.*, 35, 2218–2236, 1996.
- 5 Tuch, T. M., Haudek, A., Müller, T., Nowak, A., Wex, H., and Wiedensohler, A.: Design and performance of an automatic regenerating adsorption aerosol dryer for continuous operation at monitoring sites, *Atmos. Meas. Tech.*, 2, 417–422, doi:10.5194/amt-2-417-2009, 2009.
- Tyson, P. D. and Preston-Whyte, R. A.: *The Weather and Climate of Southern Africa*, Oxford University Press, Cape Town, 408 pp., 2000.
- 10 Vaisala: Available at: <http://www.campbellsci.com/wxt510>, access date: 1 April 2010.
- Virkkula, A., Laakso, L., Laakso, H., Vakkari, V., Beukes, P. J., Van Zyl, P., Pienaar, J. J., Chiloane, K., Fourier, G., Piketh, S., Tuch, T., Wiedensohler, A., and Kulmala, M.: A diluter for a PSAP at a EUCAARI-station in South Africa, European Aerosol Conference, Karlsruhe, 6–11 September, 2009, Abstract T170A19, 2009.
- 15 Wenig, M., Spichtinger, N., Stohl, A., Held, G., Beirle, S., Wagner, T., Jähne, B., and Platt, U.: Intercontinental transport of nitrogen oxide pollution plumes, *Atmos. Chem. Phys.*, 3, 387–393, doi:10.5194/acp-3-387-2003, 2003.

Table 1. Measurements.

	Measured properties	Instrument	Period
Meteorology	T , ρ , RH, WD, WS	Vaisala WXT510	Oct 2008–
	Radiation	LiCor LI-190SB	Oct 2008–
	ΔT	Rotronic MP101A	Oct 2008–
Trace gases	SO ₂	Thermo 43C	Continuous
	NO, NO _x	Thermo 42i	
	O ₃	Monitor Europe ML9810B	
	H ₂ S	Thermo model 340 and 43A	
Aerosol number size distribution	10–870 nm	SMPS	Feb 2009–
	0.3–10 μ m	GRIMM 1.108 OPC	May–Aug 2009
	0.3–2.2 μ m	GRIMM 7.309 OPC	Sep 2009–May 2010
	0.75–10 μ m	Droplet measurement technique CCNC optics	Sep 2009–
Aerosol absorption	Light absorption by PM ₁₀ -aerosol	Thermo model 5012 MAAP	Feb 2009–
	Three wavelength light absorption by PM ₁₀ -aerosol	Radiance research PSAP	Feb 2009–
Aerosol scattering	Three wavelength light scattering by PM ₁₀ -aerosol	Ecotech Aurora 3000	Feb 2009–
Aerosol optical depth		Sunphotometer	Nov 2010–
Aerosol chemical composition	PM _{2.5} , PM _{2.5–10}	Partisol	May 2009–Jan 2010, Jul 2010–
Aerosol back scattering		PollyXT Raman lidar	Dec 2010–Jan 2011

South African EUCAARI – measurements

L. Laakso et al.

Title Page

Abstract

Introduction

Conclusions

References

Tables

Figures

I◀

▶I

◀

▶

Back

Close

Full Screen / Esc

Printer-friendly Version

Interactive Discussion



South African EUCAARI – measurements

L. Laakso et al.

Table 2. Average values for selected parameters during the study.

Parameter	Unit	Whole period	Event	Rain	Clean
Temperature	[°C]	11.8	13.5	7.3	7.7
RH	[%]	48.2	29.3	86.3	82.1
N_{tot}	[cm^{-3}]	5840	11 960	590	340
PM ₁₀ (calculated from volume)	[$\mu\text{g m}^{-3}$]	56	114	7	20
Absorption coefficient	[M m^{-1}]	10	11	1	1
Scattering coefficient	[M m^{-1}]	55	57	7	11
SSA	–	0.8	0.8	0.8	0.9
Ångström exponent	–	1.8	1.7	1.5	1.9

Title Page

Abstract

Introduction

Conclusions

References

Tables

Figures

◀

▶

◀

▶

Back

Close

Full Screen / Esc

Printer-friendly Version

Interactive Discussion



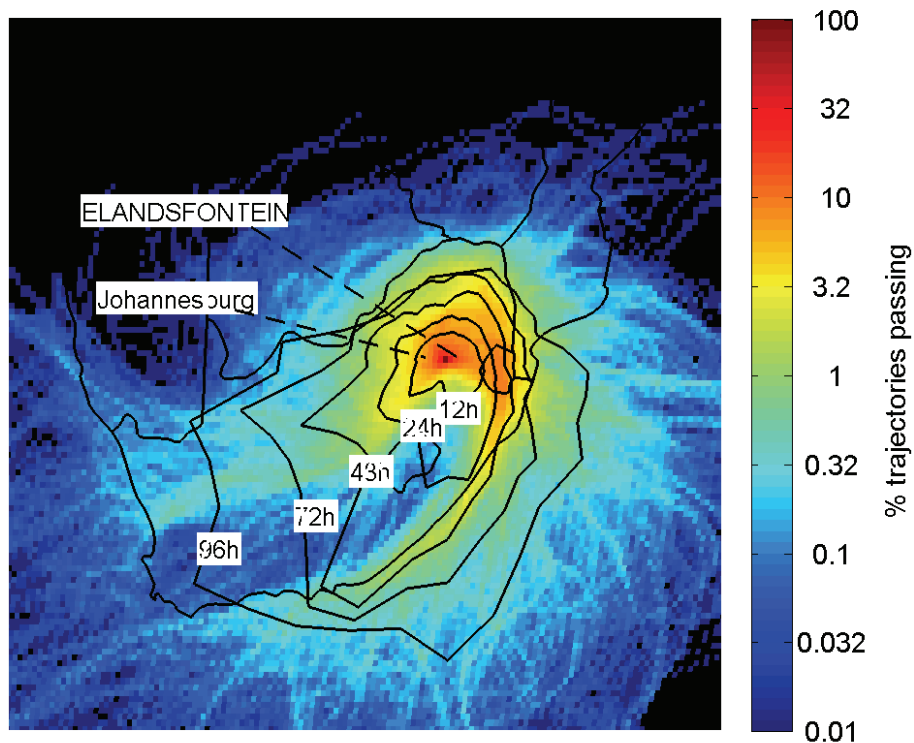


Fig. 1. Overlay back trajectory plot for the period 2007–2008 showing the percentage of trajectories arriving at Elandsfontein passing over specific areas. The black lines are contour time lines that indicate the average trajectory position in each direction at a given time (12, 24, 48, 72 and 96 h).

**South African
EUCAARI –
measurements**

L. Laakso et al.

Title Page

Abstract

Introduction

Conclusions

References

Tables

Figures

◀

▶

◀

▶

Back

Close

Full Screen / Esc

Printer-friendly Version

Interactive Discussion



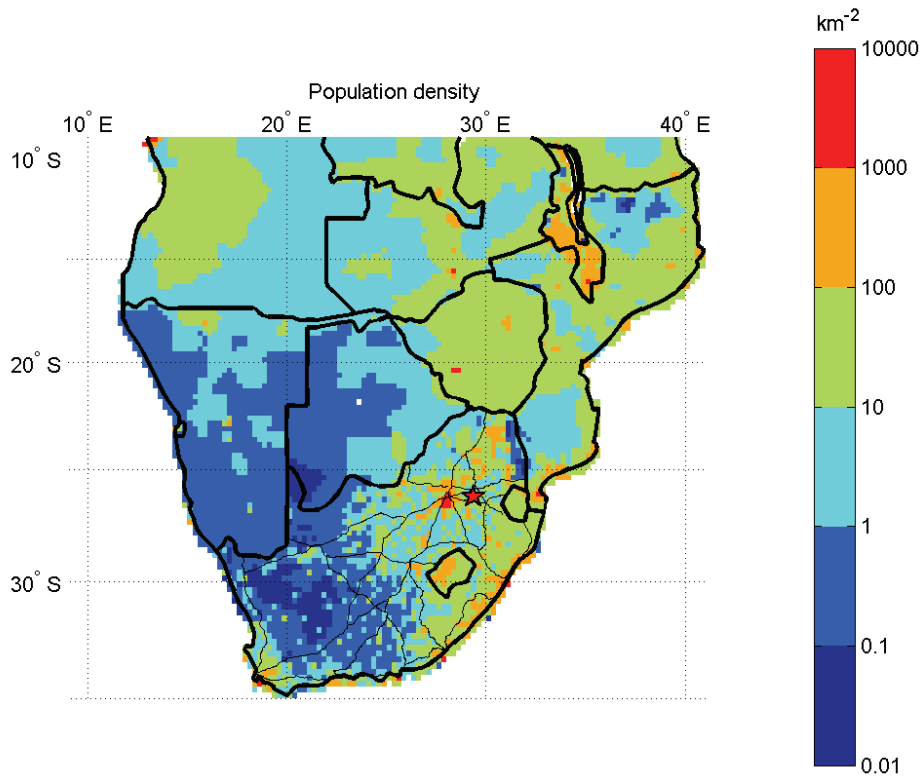


Fig. 2. Population density over Southern Africa (CIESIN, 2010). In South Africa the main national roads are also shown. The measurement site is indicated with a red star. The population hot-spot west of the measurement site is the Gauteng metropolitan area consisting of Pretoria, Johannesburg and the Vaal Triangle.

**South African
EUCAARI –
measurements**

L. Laakso et al.

Title Page

Abstract

Introduction

Conclusions

References

Tables

Figures

◀

▶

◀

▶

Back

Close

Full Screen / Esc

Printer-friendly Version

Interactive Discussion



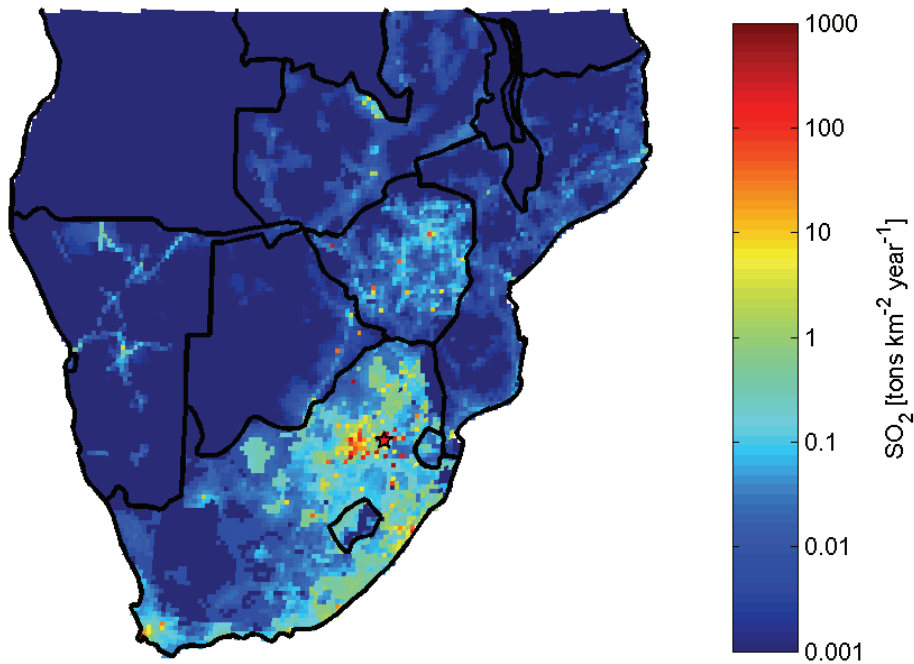


Fig. 3. Total SO₂-emissions based on SAFARI2000 emission inventory (Fleming and van der Merwe, 2004). The measurement site is indicated with a red star.

**South African
EUCAARI –
measurements**

L. Laakso et al.

Title Page

Abstract Introduction

Conclusions References

Tables Figures

◀ ▶

◀ ▶

Back Close

Full Screen / Esc

Printer-friendly Version

Interactive Discussion



South African EUCAARI – measurements

L. Laakso et al.

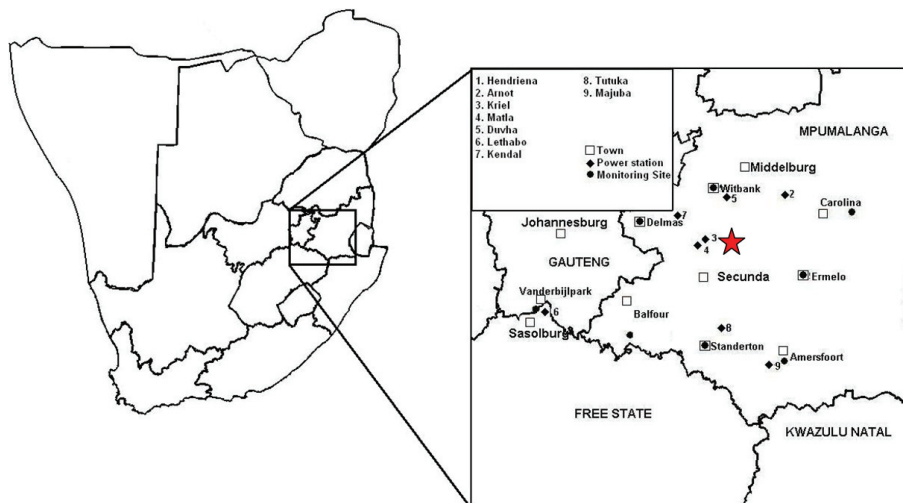


Fig. 4. Surroundings of the measurement site. Measurement site is indicated by a star.

Title Page

Abstract

Introduction

Conclusions

References

Tables

Figures

◀

▶

◀

▶

Back

Close

Full Screen / Esc

Printer-friendly Version

Interactive Discussion



**South African
EUCAARI –
measurements**

L. Laakso et al.

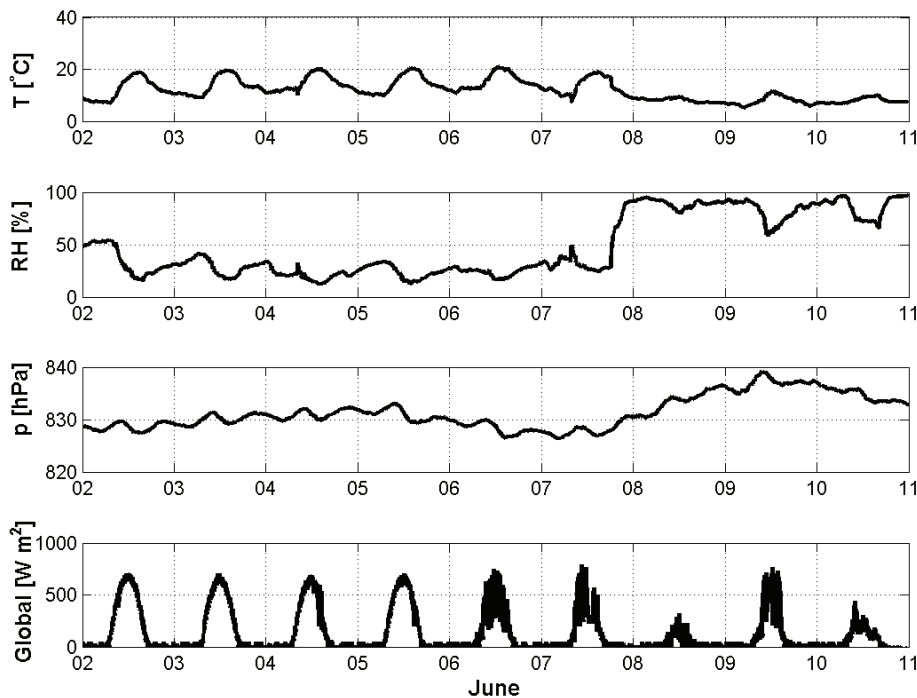


Fig. 5. Temperature (T), relative humidity (RH), pressure (p) and global radiation during 2–10 June 2009.

[Title Page](#)[Abstract](#)[Introduction](#)[Conclusions](#)[References](#)[Tables](#)[Figures](#)[◀](#)[▶](#)[◀](#)[▶](#)[Back](#)[Close](#)[Full Screen / Esc](#)[Printer-friendly Version](#)[Interactive Discussion](#)

South African
EUCAARI –
measurements

L. Laakso et al.

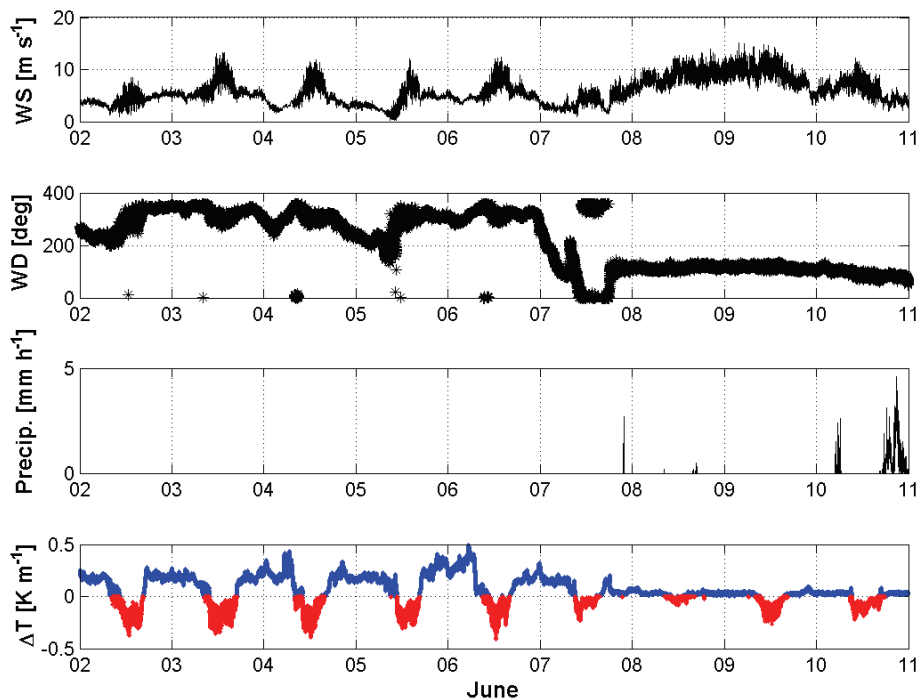


Fig. 6. Wind speed (WS), wind direction (WD), precipitation and potential temperature gradient (ΔT , a rough measure of vertical mixing) during 2–10 June 2009.

[Title Page](#)[Abstract](#)[Introduction](#)[Conclusions](#)[References](#)[Tables](#)[Figures](#)[◀](#)[▶](#)[◀](#)[▶](#)[Back](#)[Close](#)[Full Screen / Esc](#)[Printer-friendly Version](#)[Interactive Discussion](#)

South African
EUCAARI –
measurements

L. Laakso et al.

Title Page

Abstract

Introduction

Conclusions

References

Tables

Figures

◀

▶

◀

▶

Back

Close

Full Screen / Esc

Printer-friendly Version

Interactive Discussion

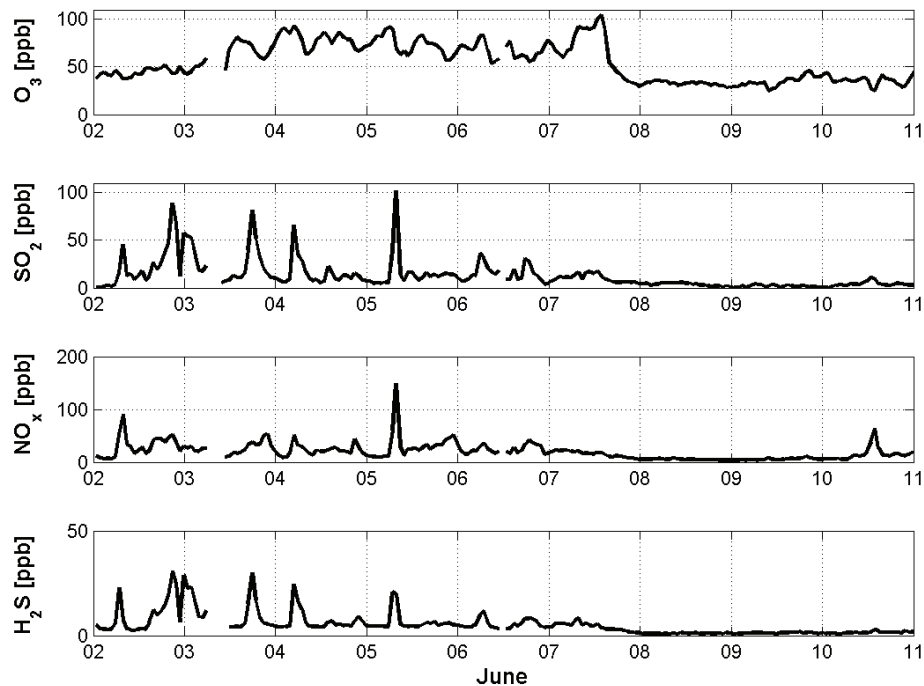


Fig. 7. Hourly-average concentrations of O_3 , SO_2 , NO_x and H_2S during 2–10 June 2009.

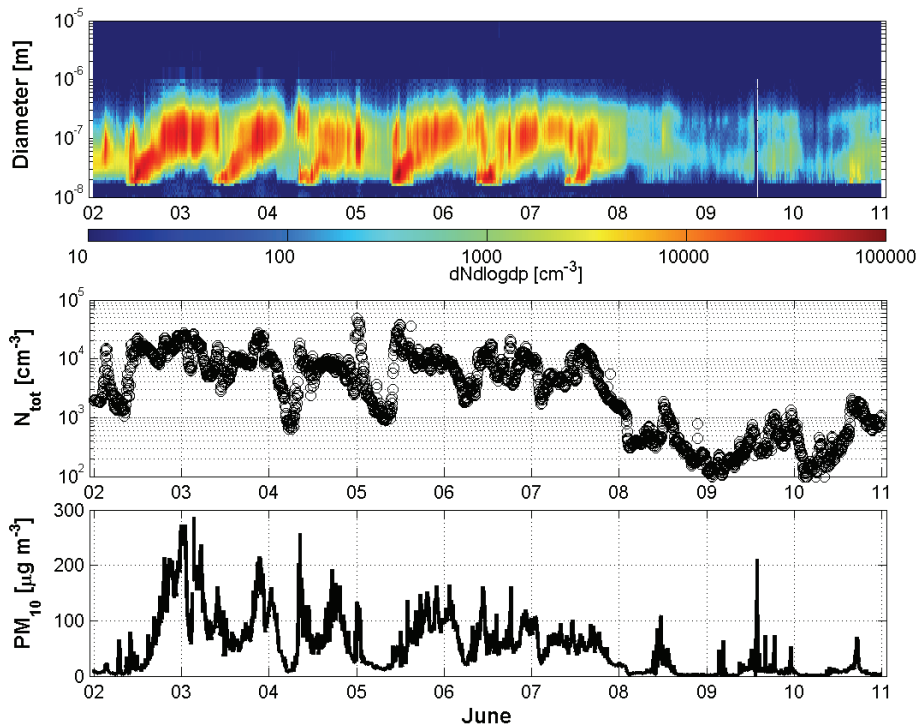


Fig. 8. Particle number size distribution and total particle number for size range 0.017–10 μm and the PM_{10} -mass concentration calculated from the particle volume (assuming particle density of 2000 kg m^{-3}) during 2–10 June 2009.

South African
EUCAARI –
measurements

L. Laakso et al.

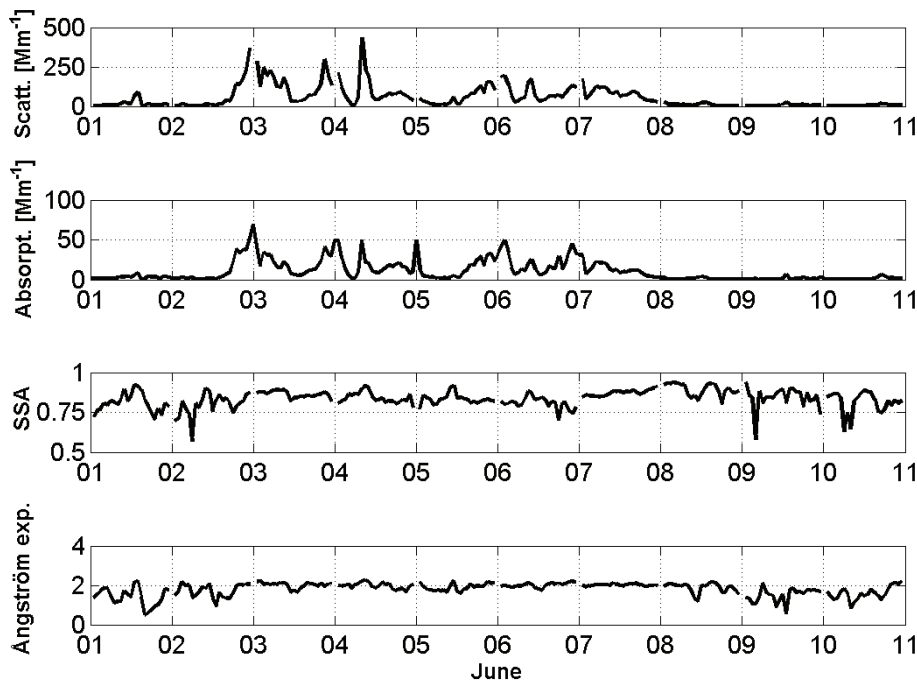


Fig. 9. Scattering and absorption coefficients, single-scattering albedo (SSA) at $\lambda=637$ nm and Ångström exponent of scattering (\AA) calculated over the wavelength range 450–700 nm for particle diameters $<10\ \mu\text{m}$ during 2–10 June 2009.

[Title Page](#)[Abstract](#)[Introduction](#)[Conclusions](#)[References](#)[Tables](#)[Figures](#)[◀](#)[▶](#)[◀](#)[▶](#)[Back](#)[Close](#)[Full Screen / Esc](#)[Printer-friendly Version](#)[Interactive Discussion](#)

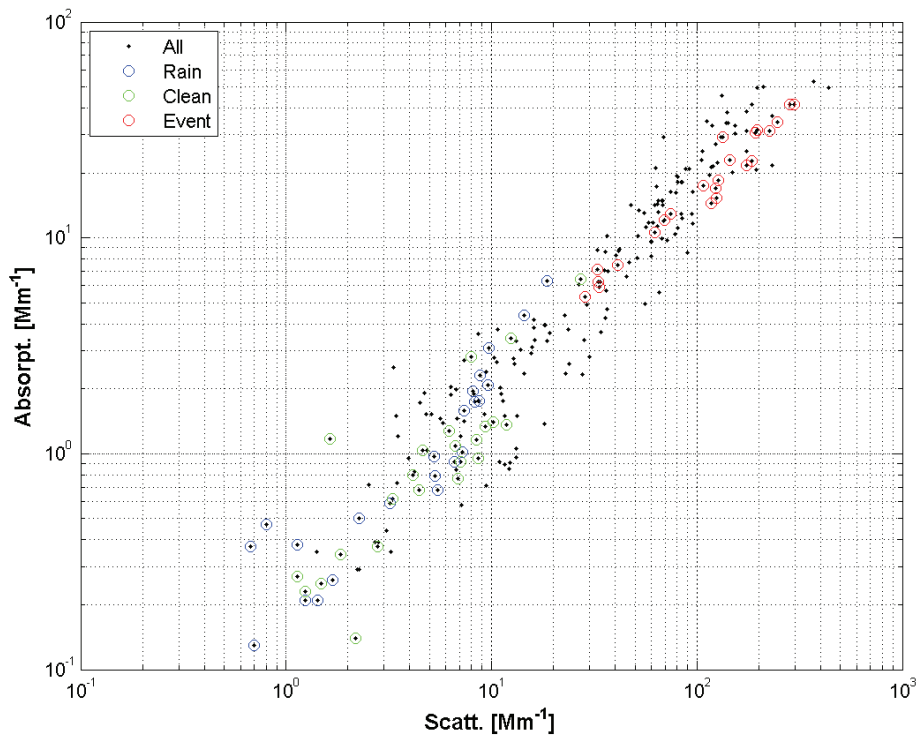


Fig. 10. Light absorption versus light scattering due to aerosol particles for the whole period and for a rainy day (10 June), clean air injection from East (9 June) and new particle formation (3 June).

**South African
EUCAARI –
measurements**

L. Laakso et al.

Title Page	
Abstract	Introduction
Conclusions	References
Tables	Figures
◀	▶
◀	▶
Back	Close
Full Screen / Esc	
Printer-friendly Version	
Interactive Discussion	



South African
EUCAARI –
measurements

L. Laakso et al.

Title Page

Abstract

Introduction

Conclusions

References

Tables

Figures

◀

▶

◀

▶

Back

Close

Full Screen / Esc

Printer-friendly Version

Interactive Discussion

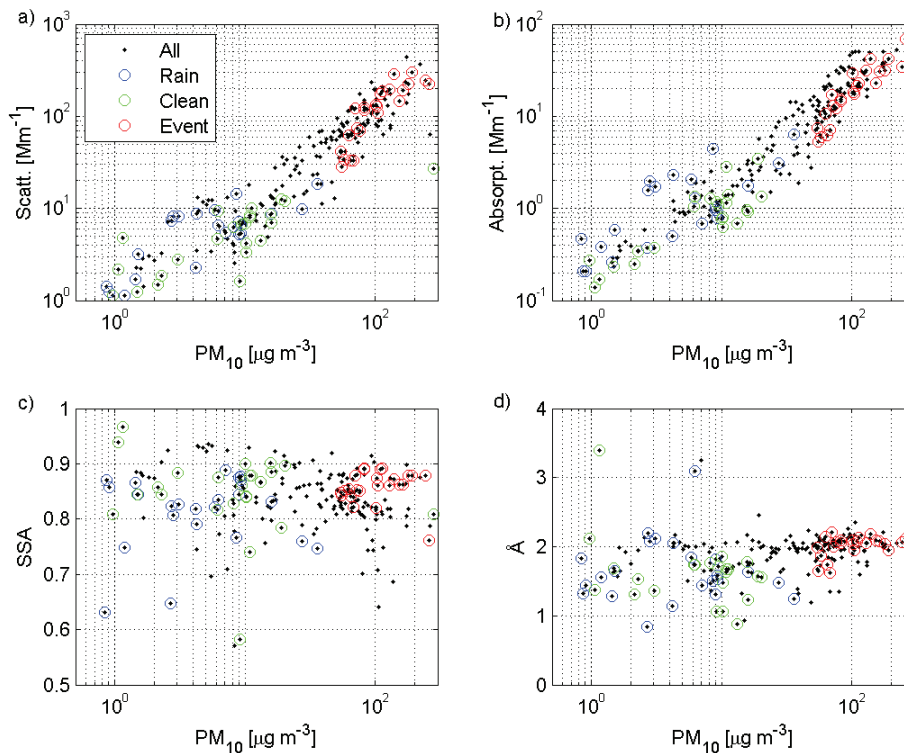


Fig. 11. (a) Scattering coefficient; (b) absorption coefficient; (c) Single scattering albedo; and (d) Ångström exponent as a function PM_{10} concentration. The classification is as in Fig. 9.

South African
EUCAARI –
measurements

L. Laakso et al.

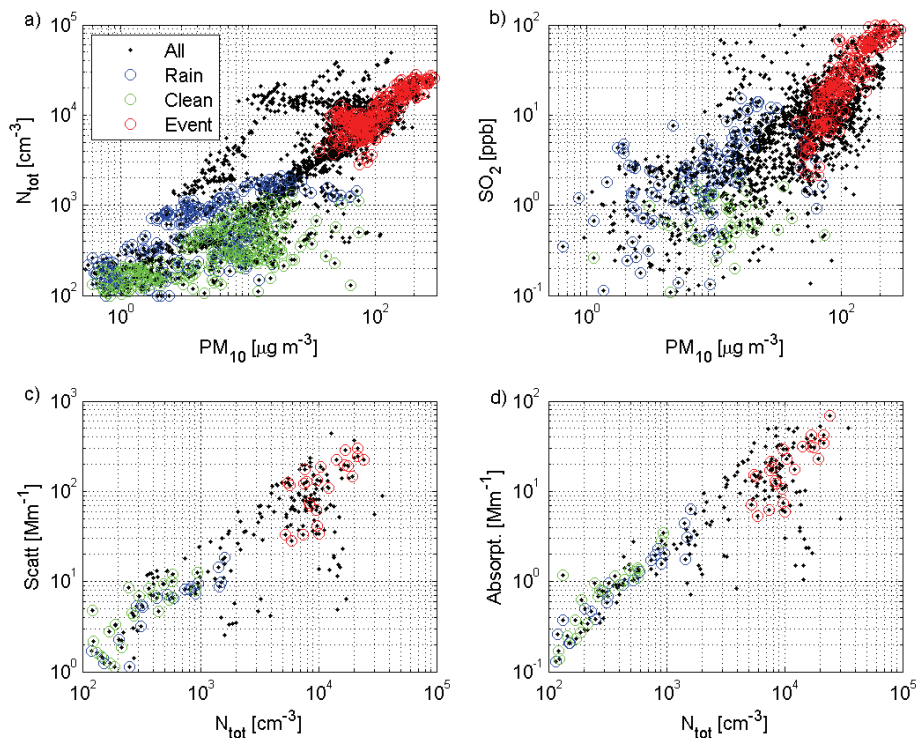


Fig. 12. (a) particle total number and (b) SO₂ as a function of PM₁₀; (c) scattering coefficient and (d) absorption coefficient as a function of total number of particles. The classification is as in Fig. 9.

Title Page

Abstract

Introduction

Conclusions

References

Tables

Figures

◀

▶

◀

▶

Back

Close

Full Screen / Esc

Printer-friendly Version

Interactive Discussion

